



Sum rule comparison of narrowband and broadband sum frequency generation spectra and comparison with theory

Kai Niu^{a,b,1}, Hong-fei Wang^{c,d}, and Rudolph A. Marcus^{b,1}

Contributed by Rudolph A. Marcus; received February 5, 2024; accepted March 26, 2024; reviewed by Shaul Mukamel and Francesco Paesani

Earlier sum frequency generation (SFG) experiments involve one infrared and one visible laser, and a measurement of the intensity of the response, yielding data on the surface sensitive properties of the sample. Recently, both the real and imaginary components of the susceptibility were measured in two different sets of experiments. In one set, a broadband infrared laser was used, permitting observations at very short times, while in another set the infrared laser was narrowband, permitting higher spectral resolution. The differences in the spectrum obtained by the two will be most evident in studying narrow absorption bands, e.g., the band due to dangling OH bonds at a water interface. The direct comparisons in the integrated amplitude (sum rule) of the imaginary part of the dangling OH bond region differ by a factor of 3. Due to variations in experimental setup and data processing, corrections were made for the quartz reference, Fresnel factors, and the incident visible laser wavelength. After the corrections, the agreement differs now by the factors of 1.1 within broadband and narrowband groups and the two groups now differ by a factor of 1.5. The 1.5 factor may arise from the extra heating of the more powerful broadband laser system on the water surface. The convolution from the narrowband SFG spectrum to the broadband SFG spectrum is also investigated and it does not affect the sum rule. Theory and narrowband experiments are compared using the sum rule and agree to a factor of 1.3 with no adjustable parameters.

sum frequency generation | phase sensitive | PS-SFG | molecular dynamics simulation | SFG

Sum frequency generation (SFG) has been widely used for investigating the interfacial structures and dynamics of physical, chemical, and biological systems for more than three decades (1–7). In the SFG experiments, an infrared (ir) pulse and visible (vis) pulse are focused on the surface simultaneously. The output signal is collected at the sum frequency in the direction that conserves the momentum of the three optical fields involved (1, 8). The intensity of the SFG spectrum is proportional to the square of the second order nonlinear susceptibility, yielding a spectrum termed the intensity spectrum (9, 10).

During the SFG process, three dipole moments are involved due to the three laser pulses. The product of the three dipole moments is ensemble averaged. For centrosymmetric systems, the product of the three dipole moments contains plus and minus signs. After ensemble averaging, the resultant signal is zero. For noncentrosymmetric systems, such as quartz crystal and water surface, the SFG signal can be observed (1, 2).

Among these SFG experiments and theories, the water surface has served as a model system for comparisons and calibrations for both experiments and theories (10-17). Interest in the water surface is also related to the phenomenon of "on water" catalysis, where the dangling OH bonds at a water surface have the ability to form a hydrogen bond with a suitable organic molecule and catalyze certain organic chemical reactions (13, 18).

Besides the absolute intensity of the SFG spectrum, the real and imaginary parts of the SFG spectrum can be detected as well. In principle, the real and imaginary parts for each mode in the spectrum resulting from the homogeneous and inhomogeneous contributions can be extracted by using a fitting process, where both Lorentzian and Gaussian lineshapes are involved (19). However, for some systems, the results of the fittings do not reflect the actual distribution of the dipole moment orientation of the surface molecules and may provide misleading information and need correction for various factors (20). The phase information of the SFG spectrum has several advantages: 1) It can distinguish between the "up" and "down" orientation of molecules or functional groups at interfaces. 2) Compared with the intensity spectrum it can help distinguish between resonant peaks and nonresonant backgrounds. 3) Phase-sensitive SFG (PS-SFG) spectrum can be used for quantitative spectrometric experiments because the signal is proportional to the density or concentration of surface molecules (3, 7).

Significance

Sum frequency generation in the phase-sensitive aspect provides the surface structure and dvnamics in an amplitude-oriented manner. Recently, the experiments for the dangling OH bond of the water surface, which are measured by various arrangements of lasers, were reported by four papers and the differences between the results can be three-folds for the integrated amplitude (sum rule) of the dangling OH bond region. After correcting the experimental results according to the experimental arrangements and the data processing methodology, the agreement within the narrowband and broadband experimental groups converged within 1.1 when using the sum rule. Moreover, the agreement between experimental measurement and the theoretical calculation is converged within 1.3 for the sum rule with no adjustable parameters.

Author contributions: K.N. and R.A.M. designed research; K.N., H.-f.W., and R.A.M. performed research; K.N., H.-f.W., and R.A.M. analyzed data; and K.N., H.-f.W., and R.A.M. wrote the paper.

Reviewers: S.M., University of California Irvine; and F.P., University of California, San Diego.

The authors declare no competing interest.

Copyright © 2024 the Author(s). Published by PNAS. This open access article is distributed under Creative Commons Attribution-NonCommercial-NoDerivatives License 4.0 (CC BY-NC-ND).

¹To whom correspondence may be addressed. Email: drniukai@gmail.com or ram@caltech.edu.

This article contains supporting information online at https://www.pnas.org/lookup/suppl/doi:10.1073/pnas. 2402550121/-/DCSupplemental.

Published May 1, 2024.

In the PS-SFG experimental arrangement, a collinear beam geometry of the incident ir and vis pulses is used. With the aid of a silica phase modulator, both the amplitude and the phase of the SFG spectrum can be measured (21-23). Several scans are then performed when measuring the phase for each data point. Another way of obtaining the phase information and the absolute intensity utilizes a noncollinear experimental arrangement, termed heterodyne-detected vibrational SFG (HD-SFG) (15–17, 24–26). In HD-SFG experiments, the incident pulses have different angles or collinearly with respect to the surface normal of the sample. The SFG pulse from the sample passes through a silica plate to construct a time delay relative to the incident ir and vis pulses. Then, the SFG signal is derived by applying a filter function to the whole signal which has the ir, vis, and SFG pulses. After a Fourier-Laplace transformation of the time-domain SFG signal, the frequency domain complex SFG spectrum can be derived. The differences in the spectrum obtained by the two methods will be most evident in the study of narrow absorption bands, for example, the band due to dangling OH bonds at a water interface. Additionally, the measurements of the real and imaginary parts of the SFG susceptibility of an air/water surface using narrowband and broadband infrared lasers for the integrated susceptibility initially appear different from each other as described later. We introduce corrections for the differences in experimental conditions of the different experiments. We then compare these corrected integrated amplitudes with that calculated using the potential energy function in the literature.

From a theoretical point of view, the SFG spectrum is a second-order susceptibility that arises from the interactions between the incident electric fields and the molecules. Both the real and imaginary parts of the appropriate susceptibility can be obtained using the Fourier-Laplace transform of a timecorrelation function (11, 14, 16, 17, 27-33). Often, the water structures for deriving the susceptibility are calculated using a molecular dynamics (MD) simulation. In the MD simulation, ways of treating the OH bond vibrations are typically of two types: the flexible water model and the rigid water model. In the first type, the OH bond length in a water molecule varies during the MD simulation. One then sees the stretching and bending motions (6, 27-29, 31). For the second type of calculation, the internal structure of the water molecule is treated as fixed and the relative position of each atom in a molecule remains the same during the MD simulation (11, 14, 34–36). The local OH bond vibrational features are identified in the latter case by using a frequency-local electric field map. Generally speaking, most of these two water models are able to reproduce the main features of the SFG spectrum, i.e., a broad peak near 3,400 cm⁻¹ and a narrow peak near 3,700 cm⁻¹. However, the rigid water models associated with the local electric field maps have a better signal to noise resolution for the dangling OH bond peak of the SFG spectrum. We use the rigid water model in our investigation.

Sum rules can be used to check the consistency between theory and experiment (37-40). They are independent of dynamics and so do not test the latter and so are structure-focused. The consequence for the sum rule of the SFG spectrum was investigated in ref. 39 assuming a Lorentzian oscillator model. However, the sum rule of the SFG second-order effective susceptibility for a general lineshape and susceptibility has not been studied yet. We focus on this topic in the present study, and in particular for the sum rule of the dangling OH bond peak in the sum frequency generation spectrum, as a way of checking the methods for the agreement of the different experiments and as a way of checking of the approximation of the theory.

The paper is organized as follows: The basic procedure for deriving the SFG experimental data and the theory on the sum rules for both the real and imaginary parts of the SFG secondorder susceptibility are reviewed and described in Section 1. The results of the corrections of the experimental spectra and the theoretical investigations are given in Section 2. The agreement among experimental measurements and the agreement between theory and experiments are discussed in Section 3 based on the sum rule. The concluding remarks are given in Section 4.

1. Theory

1.1. Theory for Processing the SFG Experimental Data. To study the connections between the PS-SFG and HD-SFG spectra, we first give an overview on how the experimental data were processed. The effective SFG susceptibilities are derived as follows (12, 15, 23, 26). After detecting the SFG signal from the water surface, the SFG spectrum for the quartz reference for the same experimental arrangement is then measured. One obtains the ratio between the SFG spectra from the water surface and the quartz. The absolute amplitude of the SFG spectrum for the water surface is then derived by taking the product of the ratio and the susceptibility of the quartz reference. The susceptibility of the quartz reference, $\chi_{q,{\rm eff,ssp}}^{(2)}(\omega)$, can be calculated as refs. 10, 41, 42

$$\chi_{q,\text{eff,ssp}}^{(2)}(\omega) = \cos \alpha_2 L_{q,yy}(\omega) L_{q,yy}(\omega_1) L_{q,yy}(\omega_2) \chi_q l_c, \qquad \textbf{[1]}$$

where the L_q s are the Fresnel factors of the quartz for the electric fields. ω , ω_1 , and ω_2 are angular frequencies for output, vis, and ir pulses, respectively. The corresponding wavelengths are λ , λ_1 , and λ_2 . α , α_1 , and α_2 are the angles that the output, vis, and ir pulses make with the surface. χ_q is the nonlinear coefficient for the second harmonic generation of the reference quartz. l_c is the effective coherence length for the reflected SFG spectrum. $L_{q,yy}$ and l_c can be calculated using the equations in refs. 41 and 43.

In SFG experiments, for each of the three pulses, there are two independent linear polarizations, s and p, and any other linear polarization is the linear combination of the two. The s-polarization represents light whose electric field is perpendicular to the plane of incidence, which is the plane that contains the surface normal and the propagation vector of the incoming radiation. The p-polarization represents light with its electric field along the plane of incidence (44). The total number of polarization combinations is $2 \times 2 \times 2 = 8$ for the SFG process.

It is possible to categorize these eight polarization combinations into three groups according to the number of the s-polarization in each process. The processes with an odd number of s-polarization, such as spp, psp, pps, and sss, can detect the structure of surface chirality and the rubbed surface, because the s-polarization is sensitive to the dipole moment along the surface (41, 42, 45-48). These combinations can be used to study the chiral structures at the surfaces.

The polarization combinations having two ss, for example, ssp, sps, and pss, could be used for the surface structure of nonchiral systems, such as the air/water interface (12, 41, 49–52). These combinations are less sensitive to chirality, and can be used to study nonchiral surfaces. The ppp process, where no s-polarization is involved, can detect both chiral and nonchiral systems. It has more or less equal dipole moment contributions along the surface and perpendicular to the surface and it can be used together with other polarization combinations for a detailed understanding of the surface information (12, 41, 49–52).

The ssp polarization combination denotes that the SFG, vis, and ir pulses are s, s, and p polarized, respectively. In this process, the ir pulse with p polarization comes to the surface, where coherence, a transition between the ground and first excited vibrational levels, of the OH bond perpendicular to the water surface is initiated, followed by the s polarized vis pulse (2). In ssp, one observes the output SFG pulse with the s polarization. The symmetry created by this specific polarization combination allows for the detection of the hydrogen bond network for water surface with high sensitivity (12).

The effective susceptibility, $\chi_{\rm eff,ssp}^{(2)}(\omega)$, for the surface is given by refs. 41 and 43

$$\chi_{\text{eff,ssp}}^{(2)}(\omega) = \mathcal{L}\chi_{yyz}^{(2)}(\omega),$$
[2]

where $\chi_{yyz}^{(2)}$ is the molecular susceptibility. The yyz is explained in detail in Section 2B. The total Fresnel factor, \mathcal{L} , represents

$$\mathscr{L} = L_{yy}(\omega)L_{yy}(\omega_1)L_{zz}(\omega_2)\sin\alpha_2, \qquad [3]$$

where \boldsymbol{L} denotes the Fresnel factor for the respective electric field.

The effective susceptibility, $\chi^{(2)}_{\rm eff,ssp}(\omega)$, is affected by the background noise factor, $\eta_{\rm B}$, in the experimental measurement, the quartz reference factor, η_q , the total Fresnel factor ratio, η_F , and the factor of the wavelength of the vis pulse, η_{λ_1} . One can introduce $\chi'(\omega)$ to correct for those effects and so check the agreement among experiments. $\chi'(\omega)$ is given by.

$$\chi'(\omega) = \chi_{\text{eff,ssp}}^{(2)}(\omega) \eta_{\text{B}} \eta_q \eta_F \eta_{\lambda_1}.$$
 [4]

The background noise often refers to a constant contribution to a measured signal and we refer it to a factor, η_B , for convenience. It is a subtractive rather than a multiplication but can be written in terms of the latter.

The lineshape of the vis pulse may affect the lineshape of the observed SFG susceptibility as well. In broadband SFG spectrum, a Gaussian lineshape laser pulse in the frequency domain is expressed as

$$E(\omega) = E_0 e^{-\delta(\omega - \omega^{\dagger})^2},$$
 [5]

where E_0 and ω^{\dagger} are the amplitude and the center frequency of the laser pulse, respectively. The linewidth measured by the energy of the laser pulse is $\sqrt{2 \ln 2/\delta}$. The SFG spectrum from a broadband vis laser pulse involves the measurement of the intrinsic lineshape of the second-order susceptibility, $\chi_0^{(2)}(\omega)$, using a broadband laser. The $\chi^{(2)}$ can be expressed as the convolution of the laser field E with $\chi_0^{(2)}(\omega)$ (2, 4)

$$\chi_1^{(2)}(\omega) = \frac{\int_{-\infty}^{\infty} d\omega' \chi_0^{(2)}(\omega') E(\omega - \omega')}{\int_{-\infty}^{\infty} d\omega' E(\omega')},$$
 [6]

where the intrinsic lineshape of the second-order susceptibility can be seen in the narrowband SFG spectrum. Then, the lineshape of the broadband SFG spectrum can be derived using Eq. 6, and conversely. However, in reality, the SFG spectrum with narrowband vis pulse yields more detailed features of the surface information than the corresponding broadband SFG spectrum, due to high signal to noise resolution (53). Eq. 6

provides the lineshape resolution among various inputs of the visible pulse width. As the electric fields are shown in both the numerator and the denominator, we show that the convolution process does not affect the integrated amplitude of the spectrum, c.f. SIA.

1.2. Theory for the Computation of the Second-Order Molecular Susceptibility. The calculation of the susceptibility of the SFG spectrum from dangling OH bonds is described in the literature (12, 29, 35, 54, 55). In this section, we present a brief description of the relevant equations and obtain the sum rule for the SFG spectrum.

Similar to the dipole–dipole time correlation function for the ir spectrum, (56) the time-dependent correlation function for the sum frequency generation has the dipole moment and polarizability matrix elements from the same molecule and the terms from different molecules (cross terms). The total second-order susceptibility, $X_{ijk}^{(2)}(\omega)$, in the frequency domain can be expressed as (2, 35)

$$X_{ijk}^{(2)}(\omega) = -\frac{1}{2\pi\epsilon_0 k_B TA} \int_0^\infty e^{-i\omega t} \langle a_{ij}(0)\dot{\mu}_k(t)\rangle dt, \quad [7]$$

where the ϵ_0 , k_B , and T are the electric permittivity of free space, the Boltzmann constant, and the temperature, respectively. A is the illuminated surface area. a_{ij} and μ_k represent the bond polarizability and dipole moment matrix elements. Integration it by parts and yields two terms, one is a constant background term, $\chi_c^{(2)}$, and the other is a frequency-resolved term, $\chi_{ijk}^{(2)}(\omega)$. It can be expressed as

$$X_{ijk}^{(2)}(\omega) = \chi_{c}^{(2)} + \chi_{ijk}^{(2)}(\omega),$$
 [8]

where

$$\chi_{c}^{(2)} = -\frac{1}{2\pi\epsilon_{0}k_{B}TA}\langle a_{ij}(0)\mu_{k}(0)\rangle$$
 [9]

and

$$\chi_{ijk}^{(2)}(\omega) = -\frac{i\omega}{2\pi\epsilon_0 k_B TA} \int_0^\infty e^{-i\omega t} \langle a_{ij}(0)\mu_k(t)\rangle dt.$$
 [10]

For a dangling OH band, the $\mu_k(t)$ oscillates with a narrow range of frequencies centered at ω_0 , 3700 cm⁻¹. Accordingly, integrating both sides of Eq. **10** ω from $-\infty$ to ∞ and replacing the ω in the pre-exponential factor by ω_0 yields a Dirac $\delta(\omega)$ function. The error is perhaps 1% or less. One then obtains

$$\int_{-\infty}^{\infty} d\omega \chi_{ijk}^{(2)}(\omega) = 2\pi i \omega_0 \chi_c^{(2)}.$$
 [11]

Seen from Eq. 11, the sum rule of the SFG spectrum for the OH found in dangling OH shows that the integrated signal for the frequency-resolved second-order susceptibility term is not affected by the system dynamics, as is always the case for sum rule.

Expanding Eq. 10 according to the contributions from various molecules, we have

$$\chi_{ijk}^{(2)}(\omega) = -\frac{i\omega}{2\pi\epsilon_0 k_B TA} \int_0^\infty e^{-i\omega t} \sum_{I,I} \langle a_{ij}^I(0) \mu_k^J(t) \rangle dt, \quad [12]$$

where the summation is from 1 to the total number of molecules. So the resultant signal is from the combined effects of all the polarizabilities and the dipole moments within and between molecules.

The contributions of the SFG spectrum from the cross terms $(I \neq J)$ is about 20% (57). When the cross terms are ignored, Eq. 12 can be expressed as (35)

$$\chi_{ijk}^{(2)}(\omega) = -\frac{i\omega N_s}{2\pi\epsilon_0 k_B T} \int_0^\infty e^{-i\omega t} \langle a_{ij}(0)\mu_k(t)\rangle dt, \qquad [13]$$

where N_s is the surface density of molecules $N_s = N/A$. N is the number of molecules in the illuminated surface area A. a_{ij} and μ_k represent the bond polarizability, and dipole moment from the same molecule, respectively. The sum rule in Eq. 11 can be expressed accordingly,

$$\int_{-\infty}^{\infty} d\omega \chi_{ijk}^{(2)}(\omega) = -\frac{i\omega_0 N_s}{\epsilon_0 k_B T} \langle a_{ij}(0) \mu_k(0) \rangle.$$
 [14]

We used the same argument to replace ω in the prefactor as was made in Eq. 11. Projecting the OH bond dynamics from the molecule coordinates onto the lab coordinates, the second-order susceptibility, $\chi_{yyz}^{(2)}$, in Eq. 13 is expressed as (35)

$$\chi_{yyz}^{(2)}(\omega) = -iN_s \int_0^\infty e^{-i\omega t} \langle e^{i\int_0^t \omega(Q[t'])dt'} \times \{ [(a_{\parallel} - a_{\perp})(\hat{r}(0) \cdot \hat{y})^2 + a_{\perp}] \times [\hat{r}(t) \cdot \hat{z}] \} \rangle dt,$$
[15]

where $\hat{r}(t)$ is the OH bond unit vector. a_{\parallel} and a_{\perp} are the hyperpolarizabilities parallel and perpendicular to the OH bond.

The second-order susceptibilities in Eq. 13 represent the molecular susceptibilities for the electric field vibrating along the i, j, and k directions. To relate the $\chi_{ijk}^{(2)}(\omega)$ to the actual experimental arrangements, one introduces Eq. 15 into Eq. 2. The input and output angles of the laser pulses and the surfacerelated information are shown in Eq. 2.

According to Eq. 15, the SFG process has the dipole moment and polarizability matrix elements and is expressed as a spatial correlation function. In the current case, the rigid water model is used in the MD simulation. So only a small amount of computational resources are required, allowing the simulation to be performed on a personal computer in several hours. In contrast, various parameters are used for simulating the quantum vibrational behavior of the OH bond for the flexible water model MD simulation. The velocity correlation function, alternative to Eq. 7 by a different integration by parts, has been used in the flexible water model and the computation time could be saved for the total calculation processes (58, 59).

2. Results

2.1. Four Sets of Experiments Treated. The experimental PS-SFG with both the lineshape and amplitude was reported in Fig. 4A, ref. 23. Collinear beam geometry was used, where an s-polarized 532 nm vis beam and a tunable p-polarized ir beam with a 30 ps linewidth were collinearly incident on a sample at an angle 45°, and the reflected s-polarized SFG spectrum was measured (23, 60). The broadband collinear experimental assignment for the ssp SFG spectrum was used in ref. 17. The incident and output angles are 45° and the vis beam is 800 nm.

A noncollinear beam geometry with different laser widths was used to measure the ssp SFG spectrum in the respective experiments (15, 25, 26). The collinearity and noncollinearity geometries of the experimental arrangements are seen from the angles of the incident lasers, the collinear geometry being the ir and vis pulses are in the same incident angle (22). The experimental vis laser pulse wavelength, bandwidth, incident and output angles of the vis and ir laser pulses, the total Fresnel and Fresnel factors in Eq. 3, and the quartz reference values in refs. 15, 17, 23, 26 are collected in Table 1.

The wavelength, the linewidth, and the incident angle of the vis and ir in columns 2, 3, 5, and 6 in Table 1 were extracted from the respective papers (15, 17, 23, 26). The output angle of the SFG pulse in column 4 has a phase matching condition with the incident pulses, $\sin \alpha/\lambda = \sin \alpha_1/\lambda_1 + \sin \alpha_2/\lambda_2$, (51, 61) where the SFG wavelength, λ , is 2.7 μ m (3,700 cm⁻¹). The Fresnel factors and total Fresnel factors representing the projection between the molecule susceptibility and the effective susceptibility were determined from the incident, reflective, and refractive pulse angles as well as from the refractive indices of the air, water, and the surface, whose equations are given in refs. 41 and 43. The quartz reference values are collected in the last column of Table 1.

The average of total Fresnel factors used for normalizing the total Fresnel factors from the four experiments is 0.357. The η_F in Eq. 4 representing the average of total Fresnel factors divided by the total Fresnel factors in Eq. 3 for refs. 23, 26, 15, and 17 are 1.01, 0.89, 1.09, and 1.02, respectively. The susceptibility corrections according to the quartz reference denoted by η_q are 0.88, 1.17, 1.17, and 0.88 for the measurements of refs. 23, 26, 15, and 17, respectively.

The η_{λ_1} representing the efficiency of the excitation produced by the vis pulse is described in detail in *SI Appendix*, c.f. SIB. The visible wavelengths for refs. 23, 26 are 532 nm, while those utilized by refs. 15, 17 are around 800 nm. The calculated result indicates that the integrated amplitude or the sum rule of the molecular susceptibility of the former is 1.14 times that of the latter. To account for this process, the correction can be made by multiplying 1.14 by the sum rule of the 800 nm SFG spectrum. So the values for η_{λ_1} are 1.0, 1.0, 1.14, and 1.14 for the measurements in refs. 23, 26, 15, and 17.

Table 1. Experimental vis pulse wavelength and bandwidth, incident and output angles of the laser pulses for the sum frequency experiments, the Fresnel factors, the total Fresnel factors, and the quartz reference values in refs. 15, 17, 23, 26

	λ_1	Width	Ar	ngle (Degre	ee)		Fresnels			Χq
Reference	(nm)	(cm^{-1})	α	α_1	α_2	$L_{yy}(\omega)$	$L_{yy}(\omega_1)$	$L_{zz}(\omega_2)$	\mathscr{L}	$(10^{-12} \text{mV}^{-1})$
(23)	532	0.42	45	45	45	0.77	0.77	0.85	0.361	0.8 (62)
(26)	532	0.53	57.4	57.5	56.6	0.68	0.68	0.81	0.316	0.6 (63)
(15)	795	25	43.3	42	48	0.77	0.78	0.84	0.388	0.6 (63)
(17)	800	14	45	45	45	0.77	0.77	0.86	0.363	0.8 (62)

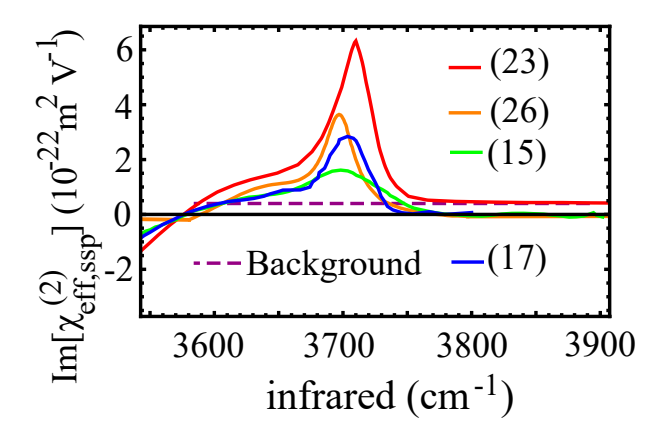


Fig. 1. Imaginary part of the effective ssp SFG spectrum from refs. 23 (red, 26 (orange), 15 (green), and 17 (blue). The purple dashed line denotes the background signal of the experimental data from ref. 23 (red) in the dangling OH bond region (from $3,600 \, \mathrm{cm}^{-1}$ to $3,900 \, \mathrm{cm}^{-1}$).

The experimental imaginary part of the effective PS-SFGs and heterodyne-detected SFGs for ssp for OH in dangling OH peak region are illustrated in Fig. 1 in red, (23) orange, (26) green, (15) and blue lines. (17) The purple dashed line represents the background of the SFG spectrum in ref. 23. The other measurements do not show the background noise explicitly. The integrated SFG spectra of the imaginary part for narrowband ir pulse and broadband ir pulse groups are collected in Table 2. The integrated susceptibility of the original data is shown in the second row. The background correction factors, $\eta_{\rm B}$ for refs. 23, 26, 15, and 17 are 0.66, 1.00, 1.00, and 1.00, respectively. The corrections are made in the cumulate form for the background contribution, quartz reference, total Fresnel factor, and the wavelength of the visible pulse are displayed from the third to the sixth rows.

In Fig. 2A, the background-removed imaginary part of $\chi'(\omega)$ of the effective ssp SFG spectrum in ref. 23 (red), the imaginary part of $\chi'(\omega)$ of the effective ssp SFG spectrum in refs. 26 (orange), 15 (green), and 17 (blue) are shown. The sum rule of the imaginary $\chi'(\omega)$ is collected in the last row in Table 2. The convolution of $\text{Im}[\chi'(\omega)]$ from narrowband SFG spectrum in ref. 26 to broadband SFG spectrum in ref. 15 according to Eq. 6 is illustrated by the orange line in Fig. 2B. The green line in Fig. 2B is the same as the orange line in Fig. 2A, representing the measurement in ref. 15. The amplitudes of refs. 15 and 17 corrected as above are times 1.5 for having a similar sum rule between the two curves.

Table 2. The sum rule of the experimental second-order susceptibility for water surface by using the narrowband ir laser (Refs. 23 and 26) and using the broadband ir laser (Refs. 15 and 17) Corrections for the background contribution, quartz reference (quartz ref), total Fresnel factors, and the visible pulse wavelength (vis wave) The unit of the integrated susceptibility is $10^{-20} \, \text{m}^2 \text{V}^{-1} \, \text{cm}^{-1}$

	Narro	Narrowband		Broadband	
Corrections	(23)	(26)	(15)	(17)	
Original	4.63	1.96	1.48	1.70	
Background	3.07	1.96	1.48	1.70	
Quartz ref	2.69	2.29	1.73	1.49	
Fresnels	2.66	2.58	1.59	1.46	
Vis Wave	2.66	2.58	1.81	1.67	

2.2. Calculation of the Sum Frequency Generation Spectrum.

The water surface structure was obtained in ref. 35 using the DL_POLY2 program, (64) where two boundary surfaces with opposite signs of the dipoles were presented. We selected the water molecules whose oxygens are in the upper half region.

To obtain the OH bond vibrational frequency from the MD simulation, we used an empirical correlation between OH bond local mode vibrational frequency in an environment and the local electric field for the extended simple point charge (65) water model given by Auer and Skinner (66). They used an equation aimed at selecting frequencies of the dangling OHs.

$$\omega_Q = (3762 - 5060E_Q - 86225E_Q^2) \text{cm}^{-1},$$
 [16]

where E_Q denotes the component of the electric field arising from the rest of the system and acting at the H atom along an OH bond Q. The electric field was calculated as allowed in three steps: (66) 1) The oxygen atom in a particular water molecule was placed at the center of a xy plane. 2) The electric field from the atoms of other water molecules at the position of the H atom was then calculated. 3) The electric field was then projected onto the OH bond.

The nonvanishing element a_{\parallel} in Eq. **15** contains a dipole moment derivative and a polarizability derivative, terms that were obtained directly from the ir and Raman spectra experiments for water vapor, (8, 35, 67–70) it has the value $5.27 \times 10^{-26} \text{m}^4 \text{V}^{-1} \text{s}^{-1}$ under the assumption that the effect of the interactions between the water molecules on these quantities was small. To allow for those interactions it might have been more appropriate to introduce instead of the OH data from H₂O vapor

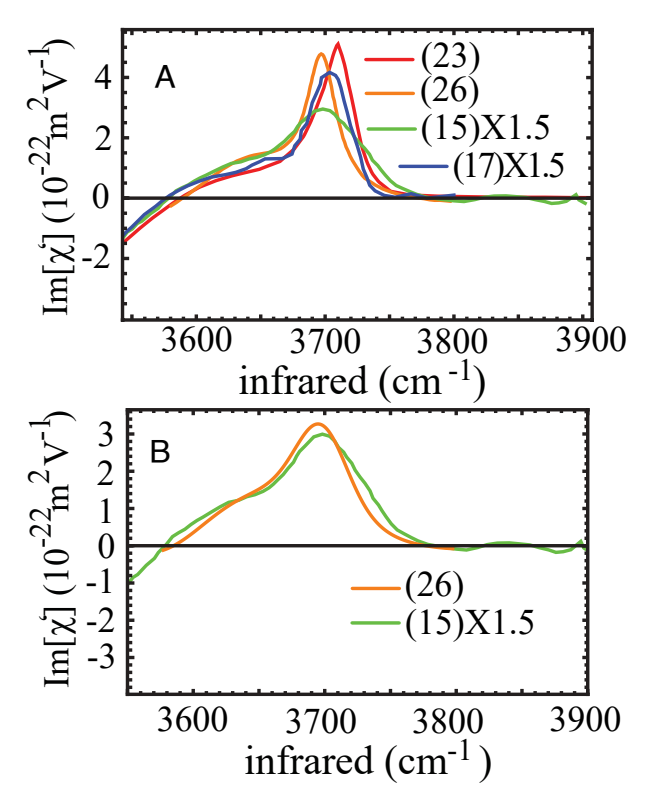


Fig. 2. (A) Background-removed imaginary part of $\chi'(\omega)$ of the effective ssp SFG spectrum in ref. 23 (red). Imaginary part of $\chi'(\omega)$ of the effective ssp SFG spectrum in ref. 26 (orange), ref. 15 (green), and ref. 26 (blue). (B) The convolved $\chi'(\omega)$ from ref. 26 (orange) and the $\chi'(\omega)$ from ref. 15 (green) in Fig. 2A. The amplitudes of $\chi'(\omega)$ of refs. 15 and 17 are times 1.5 for having a similar sum rule of the four curves. Reproduced with permissions from refs. 15, 17, and 23. Copyright 2015, 2016, and 2023, AIP Publishing. Reproduced with permission from ref. 26. Copyright 2017, American Chemical Society.

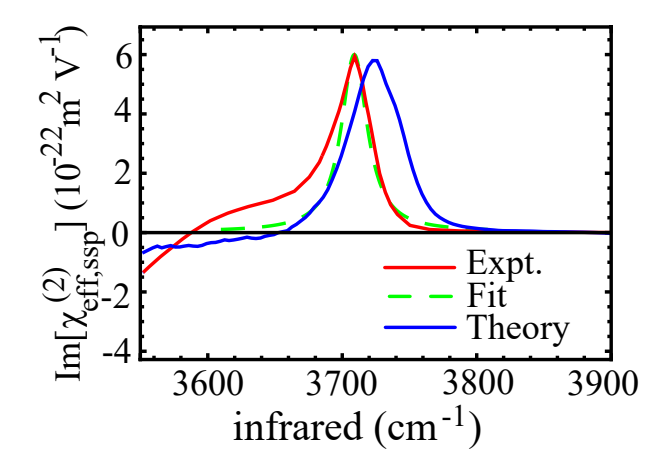


Fig. 3. The background-removed experimental imaginary part of ssp SFG spectrum in ref. 23 (red), curve of the dangling OH bond peak fitted by a Lorentzian lineshape (green dashed line), and calculated SFG spectrum (blue) for dangling OH region.

the corresponding quantities for a dangling OH bond in a water cluster (35, 71). We adopted the simplest approach using the data from H₂O vapors instead.

The calculated imaginary part of the effective ssp SFG spectrum is shown as a blue line in Fig. 3. The full width at half maximum (FWHM) and integrated amplitude (area) between 3650 and 3850 cm⁻¹ are shown in the second row in Table 3. The Fresnel factors in the calculation are taken from ref. 12. The angle of the incident ir pulse is 45° (23). The OH stretching vibrational damping factor was chosen as $\gamma_{\text{vib}} = 4 \text{ cm}^{-1}$, which corresponds to about 1 ps structure memory time in liquid water (14,72). Since the γ_{vib} is small, it has little effect on the integrated SFG spectrum, we do not refer to this value as an adjustable parameter. The laser parameters used in the calculation are given in Table 1.

3. Discussion

The overall lineshapes in the experiments for the spectra are shown in Fig. 1. One can see a 3,700 cm⁻¹ peak and a hump to the red of that peak in each experimental spectrum. The 3,700 cm⁻¹ peak is assigned as the OH in dangling OH for the water surface, where one OH bond of a water molecule points on the average to the vapor and the other OH bond of the water molecule forms a hydrogen bond with another water molecule (8, 12, 73). It has been suggested that the hump to the red of the dangling OH peak may be due to the structures of the weakly interacting OH bond and various suggestions have been made (26, 73–77). The background (purple dashed line) is treated as the experimental noise (78, 79).

Table 3. Experimental from ref. 23 and calculated ${
m Im}[\chi^{(2)}_{
m eff,ssp}]$ for the dangling OH bond region

	Peak position	Amplitude	Width	Area
Paper	(cm^{-1})	([†])	(cm ⁻¹)	([‡])
Expt.*	3709	5.9	26	2.4
Our calculation	3724	5.8	46	3.0

^{*} Background-removed spectrum in Fig. 4A in ref. 23. † The unit of the amplitude is 10^{-22} m 2 V $^{-1}$.

We first note from the comparison of the results in the second and last rows of Table 2 that the net correction for the narrowband results in the table is substantially larger than for the broadband results. A reason for any large differences among these measurements is due to the different experimental arrangements shown in Table 1. We next discuss the agreement between the narrowband and broadband SFG spectra for the imaginary part, and the agreement between experimental and calculated SFG spectra is discussed using the sum rule. The discussion of the sum rule of the real part SFG spectrum is shown in SIC.

3.1. Sum Rule Comparison between Experiments. In Eq. 4, the $\chi'(\omega)$ has been corrected for the effects arising from the experimental optical geometry, the quartz reference value, and the incident wavelength of the vis pulse. Inspection of Fig. 2A shows that the narrowband SFG spectra in refs. 23 and 26 have stronger peak intensities and have better signal to noise resolution compared with the measurement in refs. 15 and 17, while the peak amplitudes for the broadband SFG spectrum in refs. 15 and 17 have smaller amplitude and a broader lineshape. Nevertheless, the agreement among those measured susceptibilities can be checked using a sum rule after correcting for the differences in experimental arrangements.

The correction to various SFG measurements using the sum rule using Eq. 4 is detailed in Table 2. The original integrated imaginary part of the second-order susceptibilities for the 3,700 cm⁻¹ band differ by a factor of 3 comparing the largest and smallest values. The background contribution from ref. 23 is corrected in the third row. The agreement between refs. 23 and 26 is improved from a factor of 2.4 to 1.6. The agreements among all the integrated susceptibilities are improved as well. The fourth row shows the correction for the quartz reference. The agreement between the experiments in refs. 23 and 26 improves to a factor of 1.2. After the correction of the total Fresnel factors in Eq. 3 in the fifth row, the data of refs. 23 and 17 remain similar arising from the identical incident and output angles seen from Table 1. The agreement within the narrowband and the broadband groups now differ by a factor of 1.1.

As shown in the third column of Table 1, the vis pulse wavelengths are 532 nm and 800 nm for the narrowband and broadband groups, respectively. The sum frequencies in the experiments are 445 and 617 nm, respectively. When the incident laser frequency approaches the resonant frequency, the transition from the ground electronic state to the excited electronic state can be enhanced. One then expects a larger susceptibility for a larger laser frequency. Additionally, we employ a simple three-level model representing the ground electronic state, first vibrational level, and the excited electronic state for the process in SIB (2, 80, 81). It shows that the susceptibility for the 532 nm SFG sum rule is 1.14 times that of the 800 nm SFG sum rule. The corresponding corrections are shown in the last row of Table 2. The agreement between the narrowband and the broadband group becomes a factor of 1.5.

The smaller integrated signal for the broadband SFG spectrum compared with that for the narrowband SFG spectrum may be explained as follows. The absolute amplitude of the effective susceptibility may be affected by the laser power. The laser powers are 3 and 18 mW for the narrowband and broadband groups, respectively (12, 82). A more powerful laser may heat the local environment and the disorder may lower the overall SFG amplitude and have a smaller integrated signal. Another contributing factor may involve the coherence length l_c in Eq. 1. The coherence length of the quartz crystal in Eq. 1 for the

 $^{^{\}ddagger}$ The unit of the area (integrated amplitude) is $10^{-20} \text{m}^2 \text{V}^{-1} \text{cm}^{-1}$.

broadband SFG spectrum may differ from that for the narrowband SFG spectrum. We do not have the information on those aspects and we do not make corrections for such possible differences.

The conversion from narrowband to broadband SFG spectrum can be achieved by a convolution process. In the broadband SFG spectrum, first, the ir pulse is made on resonance with the vibrational transition of the local mode for the water molecule. Then, the vis pulse which is off-resonance with the transition between the ground and the excited electronic state of the water molecule creates an instant wavepacket that mimics the lineshape of the broad vis pulse. One can see the broad SFG spectrum peaks. Therefore, a broadening effect on the dangling OH peak in the broadband SFG spectrum is due to the broad vis pulse in the experimental arrangement (53, 81). In narrowband SFG spectrum, the 0.53 cm⁻¹ bandwidth in the last row of Table 1 for the vis pulse is small enough to reveal the intrinsic lineshape of the dangling OH band. Then, the $\chi'(\omega)$ from ref. 26 was convoluted with the 25 cm⁻¹ bandwidth laser pulse which was used in ref. 15. The calculated $\chi'(\omega)$ is shown as the orange line in Fig. 2*B*, while the green line is a copy of the green $\chi'(\omega)$ in Fig. 2A.

3.2. Sum Rule Comparison between Theory and Experiments.

Comparisons between the experimental (red line) and calculated (blue line) imaginary part of the effective ssp PS-SFG spectra for dangling OH region are shown in Fig. 3. The red line represents the background removed SFG spectrum from ref. 23 in Fig. 1. The positive peak has the hump around 3,640 cm⁻¹ and the dangling OH mode whose high frequency boundary is to the red of the 3,700 cm⁻¹ peak (26, 73-77). The dangling OH mode is extracted by assuming a Lorentzian lineshape (26). (green dashed line) The present paper mainly focuses on the dangling OH peak, and we compare theory and the experimental data within the green dashed line. The peak position, peak amplitude, FWHM, and the integrated amplitude of the dangling OH peak in experiment and theory are collected in Table 3. The width of the spectrum from the experiment is significantly smaller than that of the theoretical calculation. The reasons may be explained as follows. This local electric field cannot fluctuate rapidly in the current case and so it cannot yield a motional line narrowing that arises from rapid fluctuations of the neighbors of the dangling OH (motional line narrowing) (14, 71, 83). Using the sum rule, in the last column of Table 3, the integrated amplitude for the dangling OH peak from experiment and theory are calculated. One can see that the agreement between the experiment and theory is improved to a factor of 1.3 for the integrated amplitude compared to that was illustrated in Fig. 3.

In ref. 84, the phase-sensitive SFG spectrum using ab initio MD was studied. Three layers, the binding interfacial layer, diffuse layer, and bulk water, for the water surface structures were proposed to describe the surface contributions to the SFG spectra (31). In the simulations, both the lineshapes and the absolute intensities were calculated and compared with the experimental effective ssp PS-SFG spectrum. Fresnel factors and the angle of incident ir pulse do not seem to be accounted for in the effective ssp SFG calculations. Those factors do not appear to have been introduced in this interesting paper.

- 1. Y. R. Shen, The Principles of Nonlinear Optics (Wiley, New York, 1984).
- S. Mukamel, Principles of Nonlinear Optical Spectroscopy (Oxford University Press, New York, 1995)
- Y. R. Shen, Fundamentals of Sum-Frequency Spectroscopy (Cambridge University Press, Cambridge, 2016).

4. Concluding Remarks

A theory for sum rule is derived for the sum frequency generation spectrum for both the imaginary and real parts. The sum rule of the sum frequency generation represents the integrated signal of the frequency domain, which is independent of dynamics and time. Of particular interest is the sum rule involving the imaginary part of the time correlation of the polarizability and dipole moment matrix elements. Concurrently, the sum rule for the real part is indicative of the background contribution.

The sum rule is used to test the agreement of experimental results for both the noncollinear and collinear arrangements (15, 17). The sum rule is seen to provide a convincing demonstration that the four experiments from refs. 15, 17, 23, 26 have strong correlations, though the experimental arrangements are different from each other. Besides the total Fresnel factor corrections, the most important contributions for sum rule correction of the imaginary part of the ssp SFG spectrum are the background contribution and the value of the quartz reference. For converting the lineshape and the amplitude from the narrowband to the broadband SFG spectra, the convolution process plays an important role.

With no adjustable parameters, the theoretical calculation agrees very well with the lineshape and amplitude as well as the sum rule for the phase-sensitive sum frequency generation spectrum of the dangling OH bond in ref. 23.

The ssp polarizations with the advantages of revealing the surface structure information, i.e., the center frequency and amplitude for the susceptibility, are investigated and interpreted by many theory and experimental groups. For the ssp SFG spectrum of the water surface, the dangling OH and hydrogen bond regions can be extracted from the spectrum. The distribution function of the dangling OH bond can be determined from ssp and ppp spectra, or the ratio between ssp and ppp spectra. As ppp has four spectrum terms, a precise calculation of the ppp is another challenge for the molecular dynamics simulation and the theory of the second-order susceptibility.

Data, Materials, and Software Availability. The DL_POLY2.0 program was used to calculate the trajectories. All other data are included in the manuscript and/or *SI Appendix*.

ACKNOWLEDGMENTS. We gratefully acknowledge helpful discussions with Professors Y. R. Shen, Chuanshan Tian, T. Tahara, and Dr. Hui Wang. This work was supported by research grants in Tianjin University of Technology and Education Nos. XJKC031432 and XJKC031532, the Tianjin Municipal Education Commission through Grant No. 2017KJ117, the open fund of the state key laboratory of molecular reaction dynamics in DICP, CAS, and at Caltech by the Office of Naval Research and the James W. Glanville Foundation. The computations presented here were conducted on the Caltech High Performance Cluster, partially supported by a grant from the Gordon and Betty Moore Foundation.

Author affiliations: ^aDepartment of Physics, School of Science, Tianjin University of Technology and Education, Tianjin 300222, China; ^bDivision of Chemistry and Chemical Engineering, Noyes Laboratory of Chemical Physics, California Institute of Technology, Pasadena, CA 91125; ^cDepartment of Chemistry, School of Science, Westlake University, Hangzhou 310030, China; and ^dInstitute of Natural Sciences, Westlake Institute for Advanced Study, Hangzhou 310024, China

H. F. Wang, Sum frequency generation vibrational spectroscopy (SFG-VS) for complex molecular surfaces and interfaces: Spectral lineshape measurement and analysis plus some controversial issues. *Prog. Surf. Sci.* 91, 155–182 (2016).

S. Nihonyanagi, S. Yamaguchi, T. Tahara, Ultrafast dynamics at water interfaces studied by vibrational sum frequency generation spectroscopy. Chem. Rev. 117, 10665-10693 (2017).

- F. Tang et al., Molecular structure and modeling of water-air and ice-air interfaces monitored by sum frequency generation. Chem. Rev. 120, 3633-3667 (2020).
- S. Yamaguchi, T. Otosu, Progress in phase-sensitive sum frequency generation spectroscopy. Phys. Chem. Chem. Phys. 23, 18253-18267 (2021).
- Q. Du, R. Superfine, E. Freysz, Y. R. Shen, Vibrational spectroscopy of water at the vapor/water interface. Phys. Rev. Lett. 70, 2313-2316 (1993).
- Y. R. Shen, Surface spectroscopy by nonlinear optics T. W. H. Enrico Fermi, M. Inguscio, Eds. (The Netherlands: North Holland, Amsterdam, 1994)
- R. R. Feng, Y. Guo, L. Rong, L. Velarde, H. F. Wang, Consistency in the sum frequency generation intensity and phase vibrational spectra of the air/neat water interface. J. Phys. Chem. A 115, 6015-6027 (2011).
- 11. A. Morita, J. T. Hynes, A theoretical analysis of the sum frequency generation spectrum of the water surface. Chem. Phys. 258, 371-390 (2000).
- 12. X. Wei, Y. R. Shen, Motional effect in surface sum-frequency vibrational spectroscopy. Phys. Rev. Lett. 86, 4799-4802 (2001).
- 13. Y. Jung, R. A. Marcus, On the theory of organic catalysis "on water". J. Am. Chem. Soc. 129, 5492-5502 (2007).
- 14. B. M. Auer, J. L. Skinner, Vibrational sum-frequency spectroscopy of the liquid/vapor interface for dilute HOD in D20. J. Chem. Phys. 129, 214705 (2008).
- S. Nihonyanagi et al., Accurate determination of complex $\chi^{(2)}$ spectrum of the air/water interface. J. Chem. Phys. 143, 124707 (2015).
- K. Y. Chiang et al., The dielectric function profile across the water interface through surface-specific vibrational spectroscopy and simulations. Proc. Natl. Acad. Sci. U.S.A. 119, e2204156119 (2022).
- 17. X. Yu, K. Y. Chiang, C. C. Yu, M. Bonn, Y. Nagata, On the Fresnel factor correction of sum frequency generation spectra of interfacial water. J. Chem. Phys. 158, 044701 (2023).
- S. Narayan et al., On water: Unique reactivity of organic compounds in aqueous suspension. 18. Angew. Chem. Int. Ed. 44, 3275-3279 (2005).
- 19. E. A. Raymond, T. L. Tarbuck, M. G. Brown, G. L. Richmond, Hydrogen-bonding interactions at the vapor/water interface investigated by vibrational sum-frequency spectroscopy of "HOD/H2O/D2O" mixtures and molecular dynamics simulations. J. Phys. Chem. B 107, 546-556 (2003).
- Y. R. Shen, V. Ostroverkhov, Sum-frequency vibrational spectroscopy on water interfaces: Polar orientation of water molecules at interfaces. *Chem. Rev.* **106**, 1140–1154 (2006).
- 21. N. Ji, V. Ostroverkhov, C. Y. Chen, Y. R. Shen, Phase-sensitive sum-frequency vibrational spectroscopy and its application to studies of interfacial alkyl chains. J. Am. Chem. Soc. 129, 10056-10057 (2007).
- Y. R. Shen, Phase-sensitive sum-frequency spectroscopy. *Ann. Rev. Phys. Chem.* **64**, 129–150 (2013).
- S. Sun et al., Phase reference in phase-sensitive sum-frequency vibrational spectroscopy. J. Chem. Phys. 144, 244711 (2016).
- 24. S. Yamaguchi, T. Tahara, Heterodyne-detected electronic sum frequency generation: Up versus down alignment of interfacial molecules. J. Chem. Phys. 129, 101102 (2008).
- S. Yamaguchi, Development of single-channel heterodyne-detected sum frequency generation spectroscopy and its application to the water/vapor interface. J. Chem. Phys. 143, 034202 (2015).
- Y. Suzuki, Y. Nojima, S. Yamaguchi, Vibrational coupling at the topmost surface of water revealed by heterodyne-detected sum frequency generation spectroscopy. J. Phys. Chem. Lett. 8, 1396-1401 (2017).
- A. Morita, J. T. Hynes, A theoretical analysis of the sum frequency generation spectrum of the water surface. II. Time-dependent approach. J. Phys. Chem. B 106, 673-685 (2002).
- 28. A. Morita, Improved computation of sum frequency generation spectrum of the surface of water. J. Phys. Chem. B 110, 3158-3163 (2006).
- 29. A. Morita, T. Ishiyama, Recent progress in theoretical analysis of vibrational sum frequency generation spectroscopy. Phys. Chem. Chem. Phys. 10, 5801–5816 (2008).
- 30. R. Zheng, W. Wei, Y. Sun, K. Song, Q. Shi, Theoretical study of vibrational energy transfer of free OH groups at the water-air interface. J. Chem. Phys. 144, 144701 (2016).
- 31. S. Pezzotti, D. R. Galimberti, M. P. Gaigeot, 2D H-Bond network as the topmost skin to the air/water interface. J. Phys. Chem. Lett. 8, 3133-3141 (2017).
- 32. B. Das, A. Chandra, Effects of stearyl alcohol monolayer on the structure, dynamics and vibrational sum frequency generation spectroscopy of interfacial water. Phys. Chem. Chem. Phys. 24, 7374-7386 (2022).
- R. H. Zheng, F. Q. Dong, W. M. Wei, W. Z. Guan, Doubly resonant sum-frequency vibrational spectroscopy of 1,1'-Bi-2-naphthol chiral solutions due to the nonadiabatic effect. J. Phys. Chem. B 126, 1558-1565 (2022).
- 34. Y. Ni, J. L. Skinner, Communication: Vibrational sum-frequency spectrum of the air-water interface, revisited. J. Chem. Phys. 145, 031103 (2016).
- 35. K. Niu, R. A. Marcus, Sum frequency generation, calculation of absolute intensities, comparison with experiments, and two-field relaxation-based derivation. Proc. Natl. Acad. Sci. U.S.A. 117, 2805-2814 (2020).
- S. Yamaguchi, T. Takayama, T. Otosu, Appraisal of TIP4P-type models at water surface. J. Chem. Phys. 159, 171101 (2023)
- J. Hirschfelder, C. Curtiss, R. Bird, Molecular Theory of Gases and Liquids (Wiley, New York, 1954).
- M. Altarelli, D. L. Dexter, H. M. Nussenzveig, D. Y. Smith, Superconvergence and sum rules for the optical constants. Phys. Rev. B 6, 4502-4509 (1972).
- K. E. Peiponen, Sum rules for the nonlinear susceptibilities in the case of sum frequency generation. Phys. Rev. B 35, 4116-4117 (1987).
- 40. E. M. Vartiainen, K. E. Peiponen, T. Tsuboi, Analysis of coherent Raman spectra. J. Opt. Soc. Am. B 7, 722-725 (1990).
- 41. X. Wei, S. C. Hong, X. Zhuang, T. Goto, Y. R. Shen, Nonlinear optical studies of liquid crystal alignment on a rubbed polyvinyl alcohol surface. Phys. Rev. E 62, 5160-5172 (2000).
- 42. X. Wei, "Sum-frequency spectroscopic studies" (PhD thesis, Department of Physics, University of California at Berkeley, USA, 2003).
- 43. X. Zhuang, P. B. Miranda, D. Kim, Y. R. Shen, Mapping molecular orientation and conformation at interfaces by surface nonlinear optics. Phys. Rev. B 59, 12632-12640 (1999).
- Optical Society of America, Handbook of Optics: Optical Techniques and Design Principles v. 1 (McGraw-Hill Publishing, London, England, ed. 2, 1994).
- M. A. Belkin, T. A. Kulakov, K. H. Ernst, L. Yan, Y. R. Shen, Sum-frequency vibrational spectroscopy on chiral liquids: A novel technique to probe molecular chirality. Phys. Rev. Lett. 85, 4474-4477 (2000).

- 46. I. Rocha-Mendoza et al., Sum frequency vibrational spectroscopy: The molecular origins of the optical second-order nonlinearity of collagen. Biophys. J. 93, 4433-4444 (2007).
- L. M. Haupert, G. J. Simpson, Chirality in nonlinear optics. Ann. Rev. Phys. Chem. 60, 345-365
- 48. E. C. Y. Yan, L. Fu, Z. Wang, W. Liu, Biological macromolecules at interfaces probed by chiral vibrational sum frequency generation spectroscopy. Chem. Rev. 114, 8471-8498 (2014).
- W. Gan, D. Wu, Z. Zhang, R. R. Feng, H. F. Wang, Polarization and experimental configuration analyses of sum frequency generation vibrational spectra, structure, and orientational motion of the air/water interface. J. Chem. Phys. 124, 114705 (2006).
- S. Sun et al., Orientational distribution of free O-H groups of interfacial water is exponential. Phys. Rev. Lett. 121, 246101 (2018).
- H. F. Wang, W. Gan, R. Lu, Y. Rao, B. H. Wu, Quantitative spectral and orientational analysis in surface sum frequency generation vibrational spectroscopy (SFG-VS). Int. Rev. Phys. Chem. 24, 191-256 (2005).
- E. H. G. Backus, N. Garcia-Araez, M. Bonn, H. J. Bakker, On the role of Fresnel factors in sum frequency generation spectroscopy of metal-water and metal-oxide-water interfaces. J. Phys. Chem. C **116**, 23351-23361 (2012).
- L. Velarde, H. F. Wang, Unified treatment and measurement of the spectral resolution and temporal effects in frequency-resolved sum-frequency generation vibrational spectroscopy (SFG-VS). Phys. Chem. Chem. Phys. 15, 19970-19984 (2013).
- R. H. Zheng et al., Theoretical study of sum-frequency vibrational spectroscopy on limonene surface. J. Chem. Phys. 140, 104702 (2014).
- Y. R. Shen, Revisiting the basic theory of sum-frequency generation. J. Chem. Phys. 153, 180901
- D. A. McQuarrie, Statistical Mechanics (J. Wiley & Sons, New York, 1971)
- Y. Nagata, S. Mukamel, Vibrational sum-frequency generation spectroscopy at the water/lipid interface: Molecular dynamics simulation study. J. Am. Chem. Soc. 132, 6434-6442 (2010).
- T. Ohto, K. Usui, T. Hasegawa, M. Bonn, Y. Nagata, Toward ab initio molecular dynamics modeling for sum frequency generation spectra; an efficient algorithm based on surface-specific velocityvelocity correlation function. J. Chem. Phys. 143, 124702 (2015).
- Y. Nagata, T. Ohto, E. H. G. Backus, M. Bonn, Molecular modeling of water interfaces: From molecular spectroscopy to thermodynamics. *J. Phys. Chem. B* **16**, 3785 (2016). X. Xu, Y. R. Shen, C. Tian, Phase-sensitive sum frequency vibrational spectroscopic study of
- air/water interfaces: H2O, D2O, and diluted isotopic mixtures. J. Chem. Phys. 150, 144701 (2019).
- N. Bloembergen, P. S. Pershan, Light waves at the boundary of nonlinear media. Phys. Rev. 128, 606-622 (1962).
- S. Singh, Handbook of Lasers: With Selected Data on Optical Technology, R. J. Pressley, Ed. (The Chemical Rubber Co., Cleveland, Ohi, 1971), pp. 489-497.
- I. Shoji, T. Kondo, A. Kitamoto, M. Shirane, R. Ito, Absolute scale of second-order nonlinear-optical coefficients. J. Opt. Soc. Am. B 14, 2268-2294 (1997).
- W. Smith, T. R. Forester, I. T. Todorov, The DL_POLY Classic User Manual (Daresbury Laboratory, United Kingdom, 2012).
- H. J. C. Berendsen, J. R. Grigera, T. P. Straatsma, The missing term in effective pair potentials. J. Phys. Chem. 91, 6269-6271 (1987).
- B. M. Auer, J. L. Skinner, IR and Raman spectra of liquid water: Theory and interpretation. J. Chem. Phys. 128, 224511 (2008).
- M. Gussoni, Infrared intensities: A new tool in chemistry. J. Mol. Structure 141, 63-92 (1986).
- W. Hagen, A. Tielens, J. Greenberg, The infrared spectra of amorphous solid water and ice $I_{\rm c}$ between 10 and 140 K. Chem. Phys. 56, 367-379 (1981).
- W. F. Murphy, The rovibrational Raman spectrum of water vapour v₁ and v₃. Mol. Phys. 36, 727-732 (1978).
- S. A. Clough, Y. Beers, G. P. Klein, L. S. Rothman, Dipole moment of water from Stark measurements of H₂O, HDO, and D₂O. J. Chem. Phys. 59, 2254-2259 (1973).
- V. Buch et al., Sum frequency generation surface spectra of ice, water, and acid solution investigated by an exciton model. J. Chem. Phys. 127, 204710 (2007).
- J. A. McGuire, Y. R. Shen, Ultrafast vibrational dynamics at water interfaces. Science 313, 1945-1948 (2006).
- N. Ji, V. Ostroverkhov, C. S. Tian, Y. R. Shen, Characterization of vibrational resonances of watervapor interfaces by phase-sensitive sum-frequency spectroscopy. Phys. Rev. Lett. 100, 096102
- I. V. Stiopkin et al., Hydrogen bonding at the water surface revealed by isotopic dilution spectroscopy. Nature 474, 192-195 (2011).
- Y. Nagata et al., The surface roughness, but not the water molecular orientation varies with temperature at the water air interface. Phys. Chem. Chem. Phys. 17, 23559–23564 (2015).
- G. R. Medders, F. Paesani, Dissecting the molecular structure of the air/water interface from quantum simulations of the sum-frequency generation spectrum. J. Am. Chem. Soc. 138, 3912-3919 (2016)
- T. Ishiyama, Existence of weakly interacting OH bond at air/water interface. J. Chem. Phys. 152, 134703 (2020)
- X. H. Hu, F. Wei, H. Wang, H. F. Wang, α -quartz crystal as absolute intensity and phase standard in sum-frequency generation vibrational spectroscopy. J. Phys. Chem. C 123, 15071-15086 (2019).
- X. Xu, Y. R. Shen, C. Tian, Response to "Comment on 'phase-sensitive sum frequency vibrational spectroscopic study of air/water interfaces: H2O, D2O, and diluted isotopic mixtures"' [J. Chem. Phys. 152, 237101 (2020)]. J. Chem. Phys. 152, 237102 (2020).
- 80. Z. Sun, X. Qiu, J. Lu, D. H. Zhang, S. Y. Lee, Three-state model for femtosecond broadband stimulated Raman scattering. J. Raman Spectrosc. 39, 1568 (2008).
- K. Niu, S. Cong, S. Y. Lee, Femtosecond stimulated Raman scattering for polyatomics with harmonic potentials: Application to rhodamine 6G. J. Chem. Phys. 131, 054311 (2009).
- 82. S. Nihonyanagi, S. Yamaguchi, T. Tahara, Direct evidence for orientational flip-flop of water molecules at charged interfaces: A heterodyne-detected vibrational sum frequency generation study. J. Chem. Phys. 130, 204704 (2009).
- R. Kubo, M. Toda, N. Hashitsume, Statistical Physics II, Nonequilibrium Statistical Mechanics (Springer Verlag, Berlin Heidelberg, ed. 2, 1992).
- O. Kroutil, S. Pezzotti, M. P. Gaigeot, M. Předota, Phase-sensitive vibrational SFG spectra from simple classical force field molecular dynamics simulations. J. Phys. Chem. C 124, 15253-15263 (2020)